Intermodal nonlinear effects mediated optical event horizon in short-length multimode fiber

V. Mishra,[1,*] S. P. Singh,[1] R. Haldar,[2] P. Mondal,[1] and S. K. Varshney[2]
[1]*Department of Physics, IIT, Kharagpur 721302, India*
[2]*Department of Electronics & Electrical Communication Engineering, IIT, Kharagpur 721302, India*
(Received 31 January 2017; published 6 July 2017)

The group-velocity-led optical event horizon (OEH) in optical fibers provides a convenient way to efficiently control a weak dispersive pulse by a comparatively strong solitonic pulse. State-of-the-art experiments demonstrating OEH make use of two different light sources, which increases the system complexity and cost. Here, we propose an elegant and cost-effective approach to observe the OEH through intermodal nonlinear interaction between azimuthally symmetric LP_{01} and LP_{02} modes of a specially designed triple-clad multimode fiber through only a single pump. The simultaneous control over dispersion and the walk off of LP_{01} and LP_{02} modes of the designed fiber pave the way for the OEH interaction. The LP_{02} mode possesses anomalous dispersion, while the LP_{01} mode exhibits normal dispersion over the wavelength range of interest. Depending upon the location of the input pump wavelength, the LP_{02} soliton can reflect a weak copropagating LP_{01} dispersive pulse, which possesses the same carrier wavelength as the soliton. The findings of this work might be useful for all-optical switching and also for the optical transistor action, where the increased feasibility is obtained by the fact that the proposed approach does not require separate input wavelengths for the soliton and the dispersive pulse. Moreover, a tunable pump source can be used to observe either a redshift or a blueshift in the dispersive pulse.

DOI: 10.1103/PhysRevA.96.013807

I. INTRODUCTION

An optical event horizon (OEH) [1] is a phenomenon in which an intense soliton creates a strong refractive index barrier for a comparatively weak dispersive pulse propagating in the normal dispersion regime (NDR) at approximately the same group velocity as the soliton. As a result, the weak dispersive pulse is unable to penetrate the soliton and gets reflected in the temporal domain. As a consequence of the reflection, the dispersive pulse either accelerates or slows down, leading to either a redshift or blueshift in its wavelength [2] and an opposite shift in the soliton wavelength, depending upon the sign of the differential group delay (DGD) between the soliton and the dispersive pulse. The OEH lies at the heart of the continuous or stepwise blueshift of the supercontinuum (SC) spectrum in the NDR of the fiber such that the dispersive pulse emitted by the soliton itself is reflected multiple times by the soliton, leading to the continuous or stepwise blueshift of the dispersive pulse carrier wavelength [3–6]. Raman-induced redshifting and the consequent temporal delay of the soliton helps it to catch its own dispersive wave in the time domain in such a way that the dispersive wave is always temporally localized behind the soliton [4–6]. Although this effect is named dispersive-wave trapping by the soliton, its underlying mechanism is the OEH interaction occurring in a continuous fashion all along the soliton trajectory. In the frequency domain, the effect manifests in the ceaseless blueshifting of the dispersive wave all along the fiber. The redshifting soliton catches its own dispersive wave only once throughout the propagation, causing its reflection and subsequent blueshift of the dispersive wave [3]. The reflection forces the dispersive wave to be bounced temporally far from the soliton, making further reflections impossible. This leads to stepwise blueshifting of the dispersive radiation. The phenomenon has also been utilized to generate highly coherent SC by launching two separate pulses simultaneously in the fiber, one in the NDR, forming a dispersive pulse, and another in the anomalous dispersion regime (ADR) [7,8], traveling as a soliton, such that both pulses have nearly identical group velocities. An octave spanning highly coherent SC generation in a 5-μm silica strand in air was reported in [7]. Demircan *et al.* [8] extended the scheme to obtain a highly coherent SC spectrum covering the whole transparency region of silica by proposing the scheme of cascaded soliton dispersive-wave reflection in order to nullify the detrimental effects of the Raman self-frequency shift of the soliton on the OEH efficiency. In addition, the scheme enables the temporal compression of broadband SC spectra into a short pulse. The evolution of a dispersive pulse trapped in a solitonic cage is studied numerically in [9,10] and experimentally in [11]. The solitonic cage is realized by launching two temporally shifted solitons in the fiber in which the dispersive pulse is trapped between the solitons. The dispersive pulse approaches each soliton in an alternative fashion and gets reflected a number of times. This multiple-reflection phenomenon leads to the back-and-forth wavelength conversion of the dispersive pulse. The key mechanism behind the process is the OEH, which is exploited to realize all-optical switching, as demonstrated in [12,13]. The connection between the frequency shifting of a dispersive pulse at an OEH and the cascaded four-wave mixing (FWM) was established recently in [14]. Under favorable conditions, the OEH interaction also changes the soliton parameters considerably in addition to influencing the dispersive pulse. This prospect of OEH has been employed to generate optical rogue waves in [15–17].

The phenomenon of OEH can be categorized under the more general area of wave reflection. In the context of fiber Bragg gratings, the temporal reflection of a weak probe pulse by a strong pump pulse was reported in the 1990s [18,19]

*vishwatoshmishra34@gmail.com

and was named the optical push-broom effect. Recently, a considerable amount of work has been done on the temporal analog of the reflection and refraction [20,21], and it has been shown that the optical pulses undergo a change in frequency on the temporal reflection and refraction when they encounter a temporal boundary separating two different refractive-index regions. The effect is equivalent to the reflection and refraction of optical beams on the spatial boundary, which change the emergent angle (direction) of the beam. In the temporal analog, the change occurs in the frequency. The mode analysis of the temporal waveguide was reported recently in [22,23]. The reflection at the temporal boundary can be mimicked by exploiting the OEH effect, although there are also other means to establish a temporal boundary.

The OEH effect results from the cross-phase modulation (XPM) interaction between the soliton and dispersive pulse. Apart from the XPM, the soliton and the dispersive wave can also interact through FWM. The theoretical and experimental study of the phase-matching conditions and the efficiency of the nonlinear FWM interaction between the soliton and the dispersive pulse was carried out in [24,25]. A recent study [26] established the phase-matching and efficiency calculations for the FWM interaction between a soliton and a cross-polarized dispersive pulse.

The OEH interaction reported so far in the literature represents the simplest scenario, in which both the dispersive pulse and the soliton pulse belong to the same spatial mode of the waveguide. In order to achieve an OEH interaction to realize all-optical switching or optical transistor action, one has to use two different wavelengths possessing approximately the same group delay. In other words, to have an all-optical control on a pulse at a desired carrier wavelength, one has to launch a second pulse with a separate carrier wavelength, which should be selected approximately such that the condition for OEH is fulfilled. The need for two different input wavelengths adds complexity to the system and also increases the cost. However, this issue can be resolved by utilizing separate spatial modes of the fiber such that one of the modes is in the anomalous dispersion regime and the other mode exhibits normal dispersion at the desired wavelength. Depending upon the DGD between the modes, one can then launch two separate pulses that have the same carrier wavelength but belong to different modes. The initial temporal delay between these modes can be adjusted to achieve an efficient OEH interaction.

In the present work, we propose a triple-clad silica fiber (TCSF) supporting multiple modes in order to confirm that the OEH interaction between different spatial modes can indeed occur. We design the TCSF in such a way that the modes which we are interested in exhibit a walk-off length of the order of a few centimeters so that a sufficient intermodal interaction might occur between them for a femtosecond pump. Depending on the sign of the walk-off length, the dispersive pulse propagating in one of the modes gets reflected by the soliton in the other mode, leading to either a redshift or blueshift in the spectrum of the former. In some cases we also observe radiation generated at wavelengths other than that of the reflected radiation. Through our extensive numerical simulations, we investigate and confirm their origin. We also derive the phase-matching conditions (PMCs) for all the new spectral components generated in the propagation.

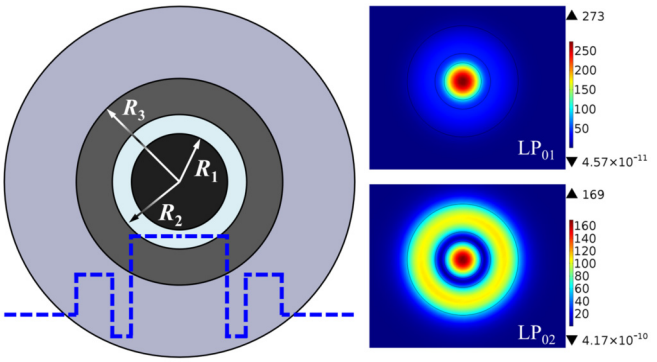

FIG. 1. Left: Schematic cross section of proposed TCSF with overlaid refractive index profile, indicated by the dashed line. Right: Mode profiles of the LP_{01} mode (top) and LP_{02} mode (bottom) at 1100 nm.

Solutions of PMCs agree well with our numerical simulation. This paper is organized as follows. In Sec. II we propose the TCSF design and perform its modal analysis. In Sec. III, we numerically solve the pulse propagation problem and study in detail the effect of various intermodal interactions. In Sec. IV, we validate our results through analytical PMC calculations. Finally, we conclude in Sec. V.

II. FIBER DESIGN AND MODAL CHARACTERISTICS

The schematic of a triple-clad silica fiber along with the refractive index profile is shown in Fig. 1. The fiber has a Ge-doped silica core with radius R_1, low-index (F-doped) silica trench with radius R_2 surrounded by a Ge-doped silica ring with radius R_3, and fused silica as cladding. The fractional molar Ge-doping concentration in the high-index silica core is represented by X_1, while it is denoted by X_2 for the Ge-doped silica ring ($X_2 < X_1$). The fluorine-doping concentration in the silica trench is fixed at 2 wt %. The effective indices of the various spatial modes guided in the structure can be manipulated by changing the dimensions of various regions and/or the Ge- and fluorine-doping concentrations.

The design we are interested in was previously fabricated in [27]. The fiber reported in [27] exhibits anomalous dispersion in the spectral region of 900–1200 nm for the higher-order LP_{02} mode, whereas the fundamental mode falls in the NDR in the aforementioned wavelength range. This fiber was subsequently used in [28] to generate femtosecond pulses near 1300 nm utilizing intermodal phase matching between an LP_{02} soliton and an LP_{11} dispersive wave. As mentioned earlier, we are interested in designing a fiber which exhibits tremendous flexibility to engineer the dispersion of the various modes and simultaneously exhibit walk-off lengths on the order of a few centimeters for the femtosecond pumping scenario. Photonic crystal fibers (PCFs) with a smaller core radius are a very promising platform for the dispersion engineering. However, for very small core area, various modes show a large DGD, which leads to an intermodal walk-off length on the order of only a few millimeters [29]. On the other hand, a large core fiber such as the graded-index fibers used in recent multimode SC generation experiments [30–32] can

TABLE I. Parameters of the TCSF.

X_1	X_2	$R_1(\mu\text{m})$	$R_2(\mu\text{m})$	$R_3(\mu\text{m})$
0.14	0.10	2	3	6

provide walk-off lengths on the order of centimeters. But for these fibers the dispersion of various modes approaches the material dispersion of the fiber material. This restricts the flexibility to selectively enhance or suppress specific intermodal nonlinear processes by dispersion control. The proposed fiber overcomes all the bottlenecks experienced with either PCFs or conventional graded-index fibers, providing both the dispersion and walk-off controls simultaneously.

The modal analysis of the TCSF was performed using the commercially available finite-element solver COMSOL MULTIPHYSICS [33]. The refractive index dispersion of various silica regions has been incorporated in the simulations [34,35]. Through extensive numerical simulations we found that for the parameters listed in Table I, the TCSF exhibits an ADR for the LP_{02} mode in the spectral region of 1000–1250 nm, while the LP_{01} mode possesses normal dispersion in the same wavelength range.

The normalized electric-field profiles of the LP_{01} and LP_{02} modes at 1100 nm are shown in Fig. 1.

Figure 2(a) shows the dispersion behavior of LP_{01} and LP_{02} modes, whereas the spectral dependence of delay for a 5-m-long TCSF is plotted in Fig. 2(b). It is clearly evident that the fiber presents dispersion suitable to launch a soliton in the LP_{02} mode, while a small fraction of the energy from the pump can be seeded to excite the dispersive pulse in the LP_{01} mode. The group velocity of the LP_{01} and LP_{02} modes matches at 1170 nm, indicating that in a spectral region around 1170 nm, a walk-off length of the order of centimeters can be achieved.

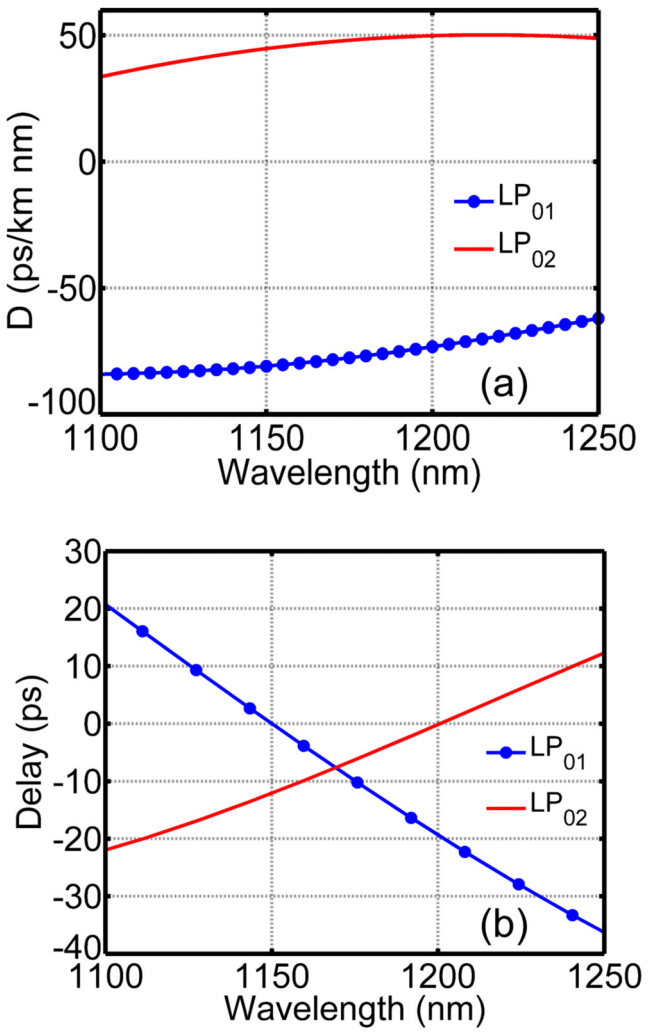

FIG. 2. (a) Dispersion characteristics of the proposed TCSF D and (b) output delay after 5 m of TCSF.

III. INTERMODAL NONLINEAR INTERACTION: ANALYSIS

We have solved the multimode generalized nonlinear Schrodinger equation (MM-GNLSE) from [36], as given in Eq. (1), where the symbol $\beta_q^{(p)}$ denotes the qth-order dispersion parameter of mode p. The parameters S^K_{plmn} and S^R_{plmn} are the spatial overlap integrals between different spatial modes predicting the strength of the Kerr and Raman interactions. For linearly polarized modes of the fibers, $S^K_{plmn} = S^R_{plmn} = S_{plmn}$.

In numerical simulations of multimode pulse propagation, we consider only azimuthally symmetric modes LP_{01} and LP_{02} of the fiber assuming that if a specific azimuthally symmetric mode is launched in a multimode fiber, the intermodal nonlinear interactions will transfer optical power to the modes belonging to only that symmetry class as the input mode. Therefore, p, l, m, and n take values of 1 or 2, representing the LP_{01} and LP_{02} modes, respectively, in our analysis. The overlap integrals of the form S_{ppqq} and S_{pqpq} describe the strength of the intermodal cross-phase modulation (IMXPM). S_{pppp} is responsible for intramodal nonlinear effects. The remaining overlap integrals represent intermodal four-wave-mixing processes (IMFWM).

$$\partial_z A_p = i\left(\beta_0^{(p)} - \beta_0^{(1)}\right)A_p - \left(\beta_1^{(p)} - \beta_1^{(1)}\right)\frac{\partial A_p}{\partial t} + \sum_{q=2}^{\infty} i^{q+1}\frac{\beta_q^{(p)}}{q!}\partial_t^q A_p + i\frac{n_2\omega_0}{c}\left(1 + \frac{i}{\omega_0}\partial_t\right) \times \sum_{l,m,n}\left[(1-f_R)S^K_{plmn}A_l A_m A_n^* + f_R A_l S^R_{plmn} \times \int_{-\infty}^{t} d\tau A_m(z,t-\tau)A_n^*(z,t-\tau)h_R(\tau)\right]. \quad (1)$$

We consider two different launching conditions, viz., (i) when the fiber is excited by a 1150-nm pump and (ii) when the pump is at 1180 nm. It should be noted that both these pumping scenarios can easily be realized using a single laser source which is tunable within a few tens of nanometers. For all calculations, we assume that the pulses are launched simultaneously in both the modes and possess a temporal duration of 100 fs. We solve Eq. (1) using the standard

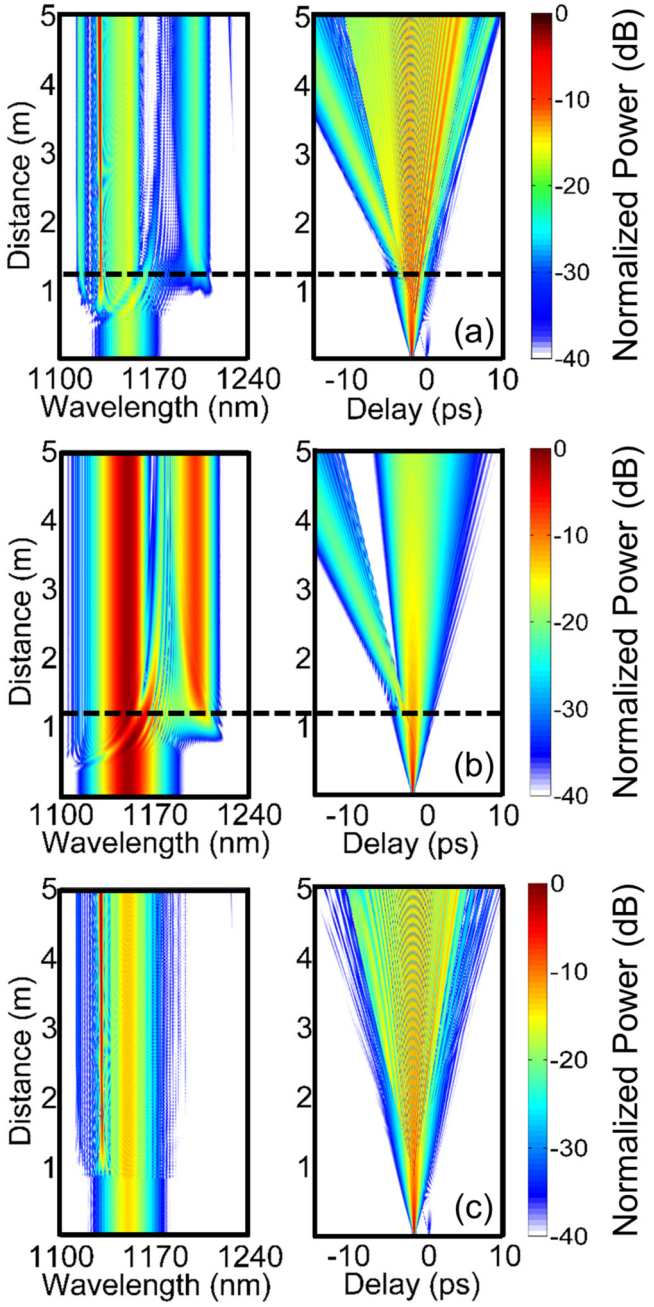

FIG. 3. (a) Spectral (left) and temporal (right) evolution of the LP_{01} mode in the TCSF when all the overlap integrals are taken into account. (b) As in (a) but all the IMFWM overlap integrals are switched off. (c) The same as (a) and (b) with all IMXPM overlap integrals switched off. The parameters of the simulation are $N_1 = 0.2$, $N_2 = 1$, $\lambda_p = 1150$ nm, and input pulse duration is 100 fs. The LP_{01} mode is launched prior to LP_{02} by 2 ps.

split-step Fourier method with an adaptive step-size algorithm [37].

The evolution of the LP_{01} mode through 5 m of the TCSF is shown in Fig. 3 (at 40-dB scale) when the light is launched at 1150 nm. The LP_{01} mode is excited with a dispersive pulse which has peak power of 110 W, corresponding to a soliton order of 0.2. A fundamental soliton with peak power of 7 kW is launched in the LP_{02} mode. At 1150 nm, the LP_{01} mode propagates at a slower group velocity than LP_{02}, which is apparent from Fig. 2(b). Therefore, in order to achieve sufficient interaction between both modes, LP_{01} is launched prior to LP_{02} by 2 ps. The corresponding evolution of the LP_{02} mode in the TCSF is shown in Fig. 4 (at 40-dB scale).

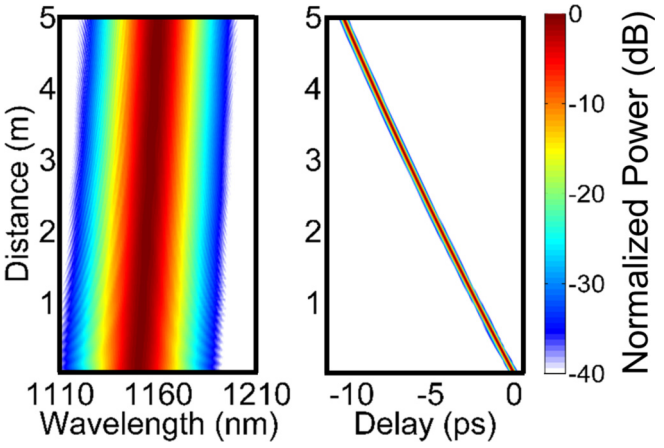

FIG. 4. Spectral (left) and temporal (right) evolution of the LP_{02} mode in the TCSF when all the overlap integrals are taken into account. The parameters of the simulation are the same as those in Fig. 3. The LP_{01} mode is launched prior to LP_{02} by 2 ps.

Figures 3(a) and 4 depict the propagation when all the overlap integrals are taken into account. From Fig. 3(a), we find that the LP_{01} mode disperses in time as it propagates. At a distance of about 50 cm, the trailing edge of the LP_{01} dispersive pulse meets the LP_{02} soliton [compare temporal evolutions of Figs. 3(a) and 4]. Afterwards, from 50 cm to 1 m, the LP_{02} soliton crosses the LP_{01} dispersive pulse in the time domain. The trailing edge of the LP_{01} dispersive pulse interacts with the soliton to give an IMFWM peak at 1130 nm at a distance of 80 cm. Finally, the leading edge of the dispersive pulse gets reflected by the LP_{02} soliton at a distance of nearly 1 m [marked with a horizontal dashed black line in Fig. 3(a)]. As a consequence of reflection, the leading edge of the dispersive pulse gets advanced in the time domain, producing a redshift. The radiation at 1200 nm is an outcome of this reflection process, i.e., OEH.

Besides those from the radiation at 1130 and 1200 nm, we also observe a quite strong peak at 1115 nm and a weak peak at 1226 nm. As confirmed through PMC calculations discussed in Sec. IV and the Appendix, the 1115-nm peak arises due to the IMFWM between the LP_{02} soliton and the LP_{01} peak generated at 1200 nm. The radiation at 1226 nm appears due to the IMFWM between the LP_{02} soliton and the residual optical power left in the LP_{01} mode at 1145 nm. Figure 4 represents the propagation of the LP_{02} soliton. It is clearly evident that the evolution of the LP_{02} soliton remains unperturbed even in the presence of the LP_{01} dispersive pulse.

Figure 3(b) represents the propagation of the LP_{01} mode when all the IMFWM terms are switched off and only IMXPM terms are retained in the calculations. We observe quite different behavior. The peaks at 1130, 1115, and 1226 nm disappear, while the peak at 1200 nm remains. This confirms that the origin of the former radiation (at 1130, 1115, and 1226 nm) is mainly due to intermodal four-wave mixing. The

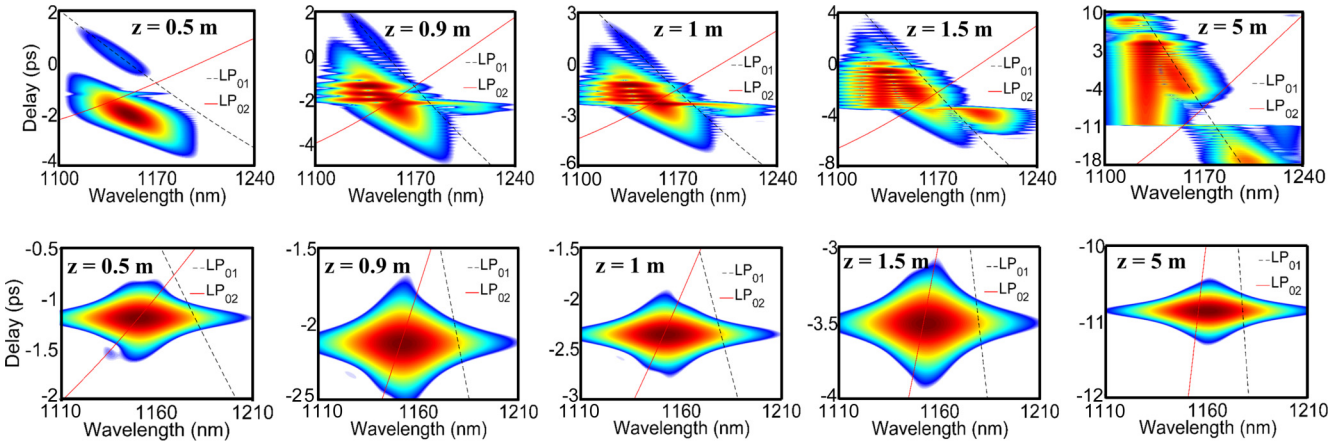

FIG. 5. Top: Spectrogram evolution for the LP_{01} mode. Bottom: Spectrogram evolution for the LP_{02} mode of the proposed TCSF. The spectrograms are taken at specified lengths shown on the plots themselves. All the overlap integrals are taken into account. Dashed black and solid red lines denote the delay profiles of the LP_{01} and LP_{02} modes, respectively.

propagation in the LP_{02} mode remains similar to that already shown in Fig. 4; hence, it is not shown separately.

Finally, to observe the effect of IMFWM terms alone on the intermodal propagation, we turn off the overlap integrals responsible for IMXPM. The propagation in the LP_{01} mode is displayed in Fig. 3(c). One can observe from Fig. 3(c) that when IMXPM terms are switched off, the radiation at 1130 nm and the weaker radiation at 1226 nm appear in the course of propagation, while the peak at 1200 nm is absent. This confirms that the peak at 1200 nm that appears as a consequence of the reflection process is due to the IMXPM interaction. The evolution of the LP_{02} mode in this case remains similar to what was already observed.

The spectrogram evolutions of the LP_{01} and LP_{02} modes corresponding to the full study of Figs. 3(a) and 4 are shown in Fig. 5. The spectrograms clearly reveal the detailed spatial and spectrotemporal structure of the output. We observe that the IMFWM peak generated at 1130 nm lags behind the LP_{02} soliton, and the IMFWM radiation at 1226 nm leads the LP_{02} soliton in the time domain. The peak at 1115 nm is delayed with respect to all other radiation generated in the LP_{01} mode. It is also observed that some residual light in the LP_{01} mode travels temporally locked with the LP_{02} soliton. The IMFWM interaction between this residual LP_{01} radiation and the LP_{02} soliton gives rise to weaker radiation at 1226 nm.

Having considered the 1150-nm pump case, we next explore the possibility of OEH interaction for the case when the LP_{01} mode travels faster than the LP_{02} mode. For this, we choose a pump wavelength of 1180 nm and launch an LP_{01} pulse at a later time than the LP_{02} pulse. The peak power in the LP_{01} mode is 110 W, corresponding to a soliton order of 0.2, whereas the peak power in the LP_{02} mode is 8 kW, forming a fundamental soliton.

Figure 6 shows the propagation of the LP_{01} mode in a 5-m-long TCSF. It is seen that the LP_{02} mode remains unaltered for the 1180-nm pump case too. From Fig. 6, we infer that the redshifting LP_{02} soliton catches up with the LP_{01} dispersive pulse at a length of 80 cm and then crosses the dispersive pulse in the time domain. At an ~1-m propagation length the LP_{01} dispersive pulse gets reflected by the LP_{02} soliton. Contrary to the case of 1150-nm pump, the dispersive pulse gets delayed after reflection, leading to its blueshift. The blueshifted radiation appears at 1140 nm. In the present scenario, no radiation is generated due to IMFWM terms, and hence, the dynamics remains unaffected even if all the IMFWM terms are switched off.

The efficiency of the reflection process in both the pumping scenarios, 1150 and 1180 nm, is computed. We observed a reflection efficiency η of 70% in the case of the 1180-nm pump. However, it is very poor (<10%) in the case of the 1150-nm pump, which is due to the maximum power carried by the IMFWM-generated peaks. This issue can be solved by increasing the soliton order of the LP_{02} mode. This would change the peak power in the LP_{02} mode, effectively modifying the PMCs. Consequently, the IMFWM peaks can be effectively suppressed.

The conversion efficiency for both the pumping scenarios can be further enhanced by increasing the pulse duration and decreasing the peak power of the LP_{01} dispersive pulse, as discussed in [38]. We can also change the initial temporal

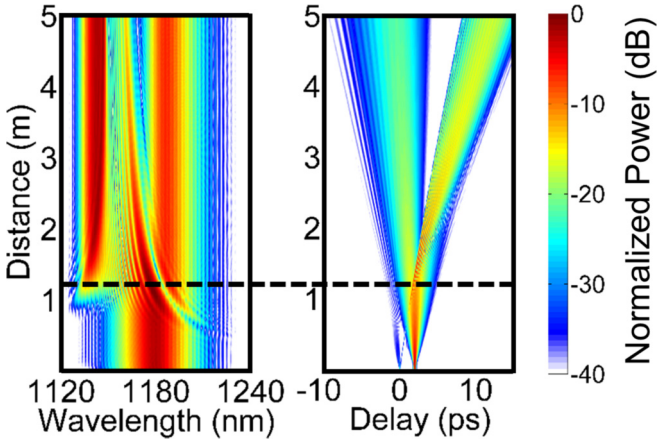

FIG. 6. Spectral (left) and temporal (right) evolution of the LP_{01} mode at the 1180-nm pump in TCSF when all the overlap integrals are taken into account. The parameters of the simulation are $N_1 = 0.2$, $N_2 = 1$, and the input pulse duration is 100 fs. The LP_{01} mode is launched after LP_{02} by 2 ps.

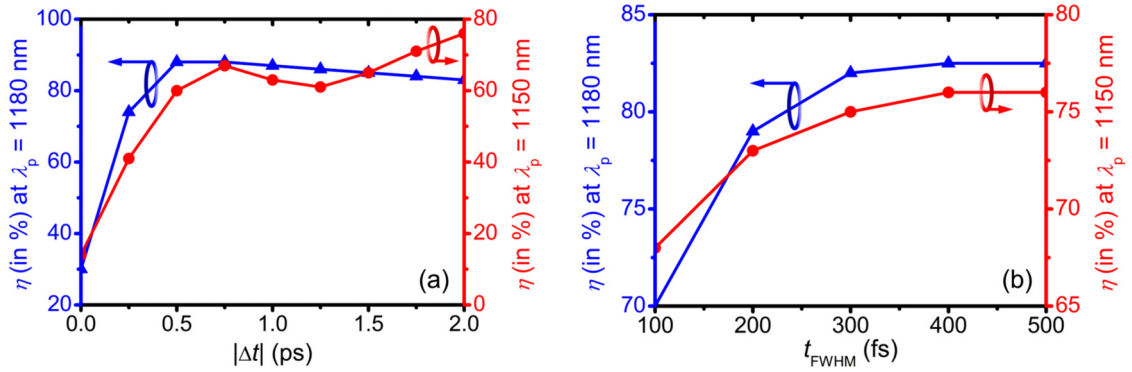

FIG. 7. (a) Variation of the conversion efficiency η with the initial absolute temporal shift $|\Delta t|$ between both modes. The FWHM pulse duration of the LP_{01} mode is set at 400 fs. (b) Variation of the conversion efficiency η with the FWHM pulse duration t_{FWHM} of the LP_{01} mode. The initial temporal shift between both pulses is set at -2 ps for the 1150-nm pump, and it equals 2 ps for the 1180-nm pump.

separation between both pulses to improve the conversion efficiency. The variation of the conversion efficiency as a function of initial temporal offset Δt and the FWHM duration of the LP_{01} pulse t_{FWHM} is shown in Figs. 7(a) and 7(b), respectively. Note that Δt is negative for the 1150-nm pump, while it is positive for the 1180-nm pump. For the 1150-nm pump, the conversion efficiency is calculated for $P_1 = 110$ W, $N_2 = 1.2$, whereas for the pump at 1180 nm, the efficiency is plotted for $P_1 = 110$ W, $N_2 = 1$. P_1 denotes the peak power of the LP_{01} pulse. The LP_{02} soliton has been assumed to have a FWHM width of 100 fs like before.

From Fig. 7, we observe that the conversion efficiency can be effectively enhanced by proper selection of the initial intermodal temporal separation. With an increase in the temporal duration of the LP_{01} dispersive pulse, the efficiency increases monotonically. However, at large temporal FWHM of the LP_{01} pulse, the efficiency tends to saturate, as depicted in Fig. 7. Note that 100% reflection can never be attained [3,14]. The reflection efficiencies observed in our study are comparable to the experimentally observed efficiencies in the single-mode OEH case [3,39].

The intermodal XPM-induced phase shift might help the formation of multimode solitons by canceling the intermodal dispersion [30,31]. In [31], the generation of intense visible peaks has been explained by assuming that the multimode pulse creates a nonlinear temporal cavity that resonantly amplifies parts of the generated continuum through the OEH effect. But it was not confirmed that the visible peaks are due to the OEH effect. In a subsequent paper [32], the authors confirmed that the underlying mechanism behind the process is the parametric instability due to the periodic intensity fluctuations in the graded-index fibers. To our understanding, this instability has no connection to the OEH interaction. Intermodal XPM-induced nonlinear interaction has also been studied theoretically [40], which induces temporal attraction between two bright (dark) solitons, while it leads to temporal attraction or repulsion between bright and dark solitons depending upon the initial temporal offset between the solitons. In a recent work [41], the polarization modulation instability between the orthogonally polarized and frequency-shifted fundamental fiber modes resulted in the generation of a dark rogue wave. The generated rogue wave was accompanied by the formation of the optical event horizon. The frequency

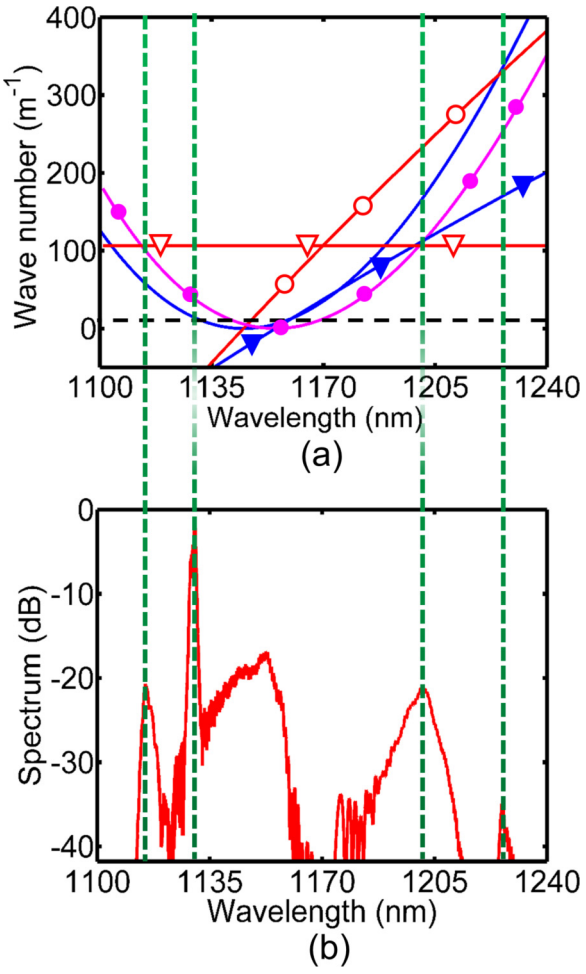

FIG. 8. (a) Solutions of the PMCs for the 1150-nm pump case and (b) spectral output in the LP_{01} mode. Solid blue curve: Left-hand side (LHS) of PMCs for $\lambda_s = 1145$ nm. Dashed black curve: Right-hand side (RHS) of PMC (2b) for $\lambda_s = 1145$ nm, $\lambda_1 = 1145$ nm. Red curve with open circles: RHS of PMC (2c) for $\lambda_s = 1145$ nm, $\lambda_1 = 1145$ nm. Solid magenta curve with solid circles: LHS of PMCs for $\lambda_s = 1155$ nm. Solid blue curve with solid triangles: RHS of PMC (2c) for $\lambda_s = 1155$ nm, $\lambda_1 = 1155$ nm. Horizontal red curve with open triangles: RHS of PMC (2a) for $\lambda_1 = 1200$ nm, $\lambda_s = 1155$ nm.

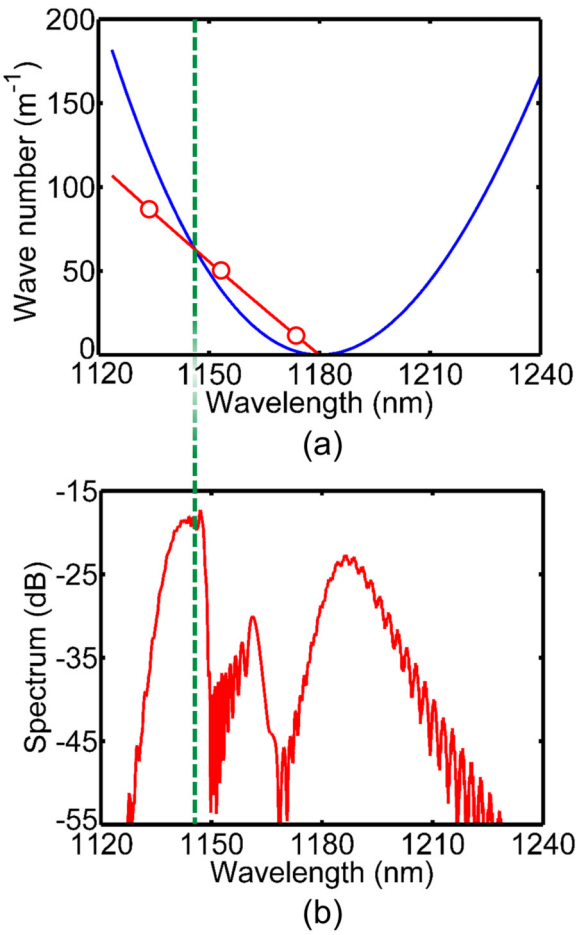

FIG. 9. (a) The solutions of the PMCs for the 1180-nm pump case and (b) spectral output in the LP_{01} mode. Solid blue curve: LHS of PMCs. Red curve with open circles: RHS of PMC (2c).

redshifts and blueshifts resulting from the OEH interaction were found to fully disappear after the rogue wave had vanished due to the transient nature of the OEH interaction.

IV. PHASE-MATCHING CONDITION

The following PMCs describing the generation in the fundamental mode can be derived by equating the phases on both sides of Eqs. (A8) and (A9) derived in the Appendix:

$$D_1(\omega_{g_1}) = D_1(\omega_1), \tag{2a}$$

$$D_1(\omega_{g_1}) = 2q_2 - D_1(\omega_1), \tag{2b}$$

$$D_1\big(\omega_{g_1}\big) = D_1(\omega_1) + (\omega_1 - \omega_{g_1})\big(\beta_1^{(1)} - \beta_1^{(2)}\big). \tag{2c}$$

The solutions of the PMCs for the 1150-nm pump case are shown in Fig. 8(a) together with the spectral output in the LP_{01} mode shown in Fig. 8(b), where λ_1 stands for the dispersive pump wavelength present in the LP_{01} mode and λ_s denotes the wavelength of the LP_{02} soliton. We observe that the PMC solutions do not match numerical simulations when we assume both the soliton and LP_{01}-mode dispersive pulse at 1150 nm, which is because the PMC derivation is based on the assumption of a cw for the dispersive pulse. However, on increasing the dispersive-pulse duration, the numerically obtained output wavelengths tend to converge to the PMC solutions which are calculated by assuming both the soliton and the dispersive pulse at the carrier wavelength of 1150 nm. To get solutions of the PMCs consistent with the numerical results, the wavelengths of the dispersive pulse pump and the soliton are slightly offset from their carrier wavelength of 1150 nm. This is reliable because both the soliton and dispersive pulse pump exhibit 3-dB bandwidths of ∼7 nm on both sides of the carrier wavelength. Moreover, in the IMFWM interactions the trailing edge of the dispersive pulse interacts with the trailing edge of the soliton, and in the reflection process the leading edge of the dispersive pulse interacts with the leading edge of the soliton. This indicates that only part of the dispersive pulse spectrum interacts with the soliton. These arguments justify why to get the correct PMC solutions for the 1150-nm pump case we have to take slightly shifted wavelengths for the dispersive pulse and the soliton. PMC solutions thus obtained agree well with the spectral radiation observed at the output. The PMC analysis for the 1180-nm pump case is also shown in Fig. 9(a), and the spectral output is shown in Fig. 9(b). We find good agreement between the PMC solution and the numerical simulation.

V. CONCLUSIONS

We have proposed a TCSF design to achieve OEH interaction in the intermodal nonlinear regime. We have observed that efficient OEH interaction is possible between a soliton and a dispersive pulse propagating at the same carrier wavelength but in a different spatial mode than the soliton itself. Depending upon the intermodal walk off between the pulses at the pump wavelength, the dispersive pulse can be redshifted or blueshifted by a proper choice of the initial delay between the pulses. The effect of various overlap integrals was also considered, and it was found that the IMXPM overlap integrals are responsible only for the OEH dynamics observed.

The spatial degree of freedom of the fiber utilized here might be useful for realizing all-optical switching [12] and optical transistor action [13] while relaxing the need for two input wavelengths to achieve the desired functionality. We believe that experimental realization of our study might pave the way for ultrafast all-optical control in robust all-fiber platforms through a single source.

ACKNOWLEDGMENTS

V.M. would like to convey his sincere thanks to CSIR-INDIA for the award of the senior research fellowship under Award No. 09/081 (1200) / 2013 - EMR - I.

APPENDIX: PMC DERIVATION

In this appendix, we derive the phase-matching conditions for the intermodal interaction between the LP_{01} dispersive pulse and the LP_{02} soliton as observed in Sec. IV. We follow an approach similar to that given in [24]. We look for the

solutions of Eq. (1) in the form

$$A_p = F_p(t_p) + g_p(z_p, t_p), \tag{A1a}$$

$$t_p = t - z\left(\beta_1^{(p)} - \beta_1^{(1)}\right), \tag{A1b}$$

$$F_p(t_p) = \psi_p(t_p) e^{i q_p z_p}, \tag{A1c}$$

where t is the time in the reference frame of the fundamental mode and t_p is the time in the reference frame of the pulse in mode p. ψ_p is the soliton solution of the single-mode GNLSE in mode p when all dispersion parameters higher than β_2 are absent; g_p accounts for all the radiation in mode p other than the soliton, including the dispersive pulse pump; z_p is the propagation distance in mode p, which is always the same as the physical distance; and q_p is the phase of the soliton in mode p.

In Eq. (1) we represent the dispersive operator by $D_p(i\partial_t)$, given as

$$D_p(i\partial_t) = \left(\beta_0^{(p)} - \beta_0^{(1)}\right) + \left(\beta_1^{(p)} - \beta_1^{(1)}\right)(i\partial_t) + \sum_{q=2}^{\infty} (i\partial_t)^q \frac{\beta_q^{(p)}}{q!}. \tag{A2}$$

We also have

$$\partial_z = \partial_{z_p} - \left(\beta_1^{(p)} - \beta_1^{(1)}\right)\partial_{t_p}, \tag{A3a}$$

$$\partial_t = \partial_{t_p}. \tag{A3b}$$

Using Eqs. (A1)–(A3) in Eq. (1) and after doing simple mathematics, we get

$$\begin{aligned} &i\left[D_p(i\partial_{t_p}) + \frac{1}{2}\beta_2^{(p)}\partial_{t_p}^2 - \left(\beta_1^{(p)} - \beta_1^{(1)}\right)(i\partial_{t_p})\right]\{\psi_p(t_p)e^{iq_p z}\} + i\frac{n_2\omega_0}{c}\sum_{l,m,n}^{p'} S_{plmn}\psi_l(t_l)\psi_m(t_m)\psi_n(t_n)e^{i(q_l+q_m-q_n)z} \\ &\quad + i\frac{n_2\omega_0}{c}\sum_{l,m,n} S_{plmn}\{g_m\psi_l(t_l)\psi_n(t_n)e^{i(q_l-q_n)z} + g_l\psi_m(t_m)\psi_n(t_n)e^{i(q_m-q_n)z} + g_n^*\psi_m(t_m)\psi_l(t_l)e^{i(q_m+q_l)z}\} \\ &= \partial_{z_p} g_p - iD_p(i\partial_{t_p})g_p - \left(\beta_1^{(p)} - \beta_1^{(1)}\right)\partial_{t_p} g_p. \end{aligned} \tag{A4}$$

The use of p' in the upper limit of the summation in the second term of Eq. (A4) signifies that the term in which all l, m, and n equal p is to be excluded from the summation. We assume that g_q consists of two parts: one is the input pump with amplitude w_q that has a frequency detuning of ω_q from the soliton carrier frequency, and the second is the generated wave represented by ϕ_q; that is,

$$g_q = w_q e^{iD_q(\omega_q)z - i\omega_q t_q} + \phi_q. \tag{A5}$$

Using Eq. (A5), Eq. (A4) can be recast as

$$\begin{aligned} &i\left[D_p(i\partial_{t_p}) + \frac{1}{2}\beta_2^{(p)}\partial_{t_p}^2 - (\beta_1^{(p)} - \beta_1^{(1)})(i\partial_{t_p})\right]\{\psi_p(t_p)e^{iq_p z}\} + i\frac{n_2\omega_0}{c}\sum_{l,m,n}^{p'} S_{plmn}\psi_l(t_l)\psi_m(t_m)\psi_n(t_n)e^{i(q_l+q_m-q_n)z} \\ &\quad + i\frac{n_2\omega_0}{c}\sum_{l,m,n} S_{plmn}\{\phi_m\psi_l(t_l)\psi_n(t_n)e^{i(q_l-q_n)z} + \phi_l\psi_m(t_m)\psi_n(t_n)e^{i(q_m-q_n)z} + \phi_n^*\psi_m(t_m)\psi_l(t_l)e^{i(q_m+q_l)z}\} \\ &\quad + i\frac{n_2\omega_0}{c}\sum_{l,m,n} S_{plmn}\{w_m\psi_l(t_l)\psi_n(t_n)e^{i[D_m(\omega_m)+q_l-q_n]z - i\omega_m t_m} + w_l\psi_m(t_m)\psi_n(t_n)e^{i[D_l(\omega_l)+q_m-q_n]z - i\omega_l t_l}\} \\ &\quad + i\frac{n_2\omega_0}{c}\sum_{l,m,n} S_{plmn} w_n\psi_m(t_m)\psi_l(t_l)e^{i[q_m+q_l-D_n(\omega_n)]z + i\omega_n t_n} \\ &= \partial_{z_p}\phi_p - i\left[D_p(i\partial_{t_p}) - i\left(\beta_1^{(p)} - \beta_1^{(1)}\right)\partial_{t_p}\right]\phi_p + i\omega_p w_p\left(\beta_1^{(p)} - \beta_1^{(1)}\right)e^{iD_p(\omega_p)z - i\omega_p t_p}. \end{aligned} \tag{A6}$$

Our case corresponds to a specific situation in which the dispersive pulse pump is in the LP_{01} mode, labeled here as 1, and the soliton is in the LP_{02} mode, labeled as 2. Therefore, we can write

$$\begin{aligned} w_q &= w_1\delta_{1q}, \\ F_q &= F_2\delta_{2q}, \\ t_q &= t_p - z\left(\beta_1^{(q)} - \beta_1^{(p)}\right). \end{aligned} \tag{A7}$$

With the help of Eqs. (A7) in Eq. (A6), separate propagation equations for mode 1 and mode 2 can be derived and are respectively given as

$$i\frac{n_2\omega_0}{c}\left[S_{1222}\psi_2^3 e^{iq_2 z}+\{S_{1212}+S_{1122}\}w_1\psi_2^2 e^{iD_1(\omega_1)z-i\omega_1 t_1}+S_{1221}w_1\psi_2^2 e^{i(2q_2-D_1(\omega_1))z+i\omega_1 t_1}\right]$$
$$=\partial_z\phi_1-iD_1(i\partial_{t_1})\phi_1-i\frac{n_2\omega_0}{c}\{S_{1212}+S_{1122}\}\psi_2^2\phi_1-i\frac{n_2\omega_0}{c}S_{1221}\phi_1^*\psi_2^2 e^{2iq_2 z}, \tag{A8}$$

$$i\left[D_2(i\partial_{t_2})+\frac{1}{2}\beta_2^{(2)}\partial_{t_2}^2-i\left(\beta_1^{(2)}-\beta_1^{(1)}\right)\partial_{t_2}\right]\{\psi_2 e^{iq_2 z}\}$$
$$+i\frac{n_2\omega_0}{c}\{S_{2212}+S_{2122}\}w_1\psi_2^2 e^{i[D_1(\omega_1)+\omega_1(\beta_1^{(1)}-\beta_1^{(2)})]z-i\omega_1 t_2}+i\frac{n_2\omega_0}{c}S_{2221}e^{i[2q_2-D_1(\omega_1)-\omega_1(\beta_1^{(1)}-\beta_1^{(2)})]z+i\omega_1 t_2}$$
$$=\partial_z\phi_2-i\left[D_2(i\partial_{t_2})-i\left(\beta_1^{(2)}-\beta_1^{(1)}\right)\partial_{t_2}\right]\phi_2-i\frac{n_2\omega_0}{c}\{S_{2212}+S_{2122}\}\psi_2^2\phi_1-i\frac{n_2\omega_0}{c}S_{2221}\phi_1^*\psi_2^2 e^{2iq_2 z} \tag{A9}$$

We represent ϕ_q as

$$\phi_q\sim e^{iD_q(\omega_{gq})z-i\omega_{gq}t_q}. \tag{A10}$$

Equating the phases on both sides of Eqs. (A8) and (A9), the following PMCs describing the generation in mode 1, which are relevant to our study, can be derived:

$$D_1(\omega_{g_1})=D_1(\omega_1), \tag{A11a}$$
$$D_1(\omega_{g_1})=2q_2-D_1(\omega_1), \tag{A11b}$$
$$D_1(\omega_{g_1})=D_1(\omega_1)+(\omega_1-\omega_{g_1})\left(\beta_1^{(1)}-\beta_1^{(2)}\right). \tag{A11c}$$

In Eqs. (A11), ω_{g_1} represents the frequency of the generated wave in mode 1, while ω_1 represents the frequency of the dispersive pulse pump present in mode 1. Equations (A11) are the same as Eqs. (2) in Sec. IV.

[1] T. G. Philbin, C. Kuklewicz, S. Robertson, S. Hill, F. König, and U. Leonhardt, Science **319**, 1367 (2008).
[2] A. Demircan, S. Amiranashvili, and G. Steinmeyer, Phys. Rev. Lett. **106**, 163901 (2011).
[3] S. F. Wang, A. Mussot, M. Conforti, A. Bendahmane, X. L. Zeng, and A. Kudlinski, Phys. Rev. A **92**, 023837 (2015).
[4] A. V. Gorbach and D. V. Skryabin, Nat. Photonics **1**, 653 (2007).
[5] S. P. Singh, V. Mishra, and S. K. Varshney, J. Opt. Soc. Am. B **33**, D65 (2016).
[6] J. C. Travers and J. R. Taylor, Opt. Lett. **34**, 115 (2009).
[7] A. Demircan, S. Amiranashvili, C. Brée, and G. Steinmeyer, Phys. Rev. Lett. **110**, 233901 (2013).
[8] A. Demircan, S. Amiranashvili, C. Brée, U. Morgner, and G. Steinmeyer, Opt. Express **22**, 3866 (2014).
[9] A. V. Yulin, R. Driben, B. A. Malomed, and D. V. Skryabin, Opt. Express **21**, 14481 (2013).
[10] R. Driben, A. V. Yulin, A. Efimov, and B. A. Malomed, Opt. Express **21**, 19091 (2013).
[11] S. F. Wang, A. Mussot, M. Conforti, X. L. Zeng, and A. Kudlinski, Opt. Lett. **40**, 3320 (2015).
[12] N. Nishizawa and T. Goto, Opt. Express **11**, 359 (2003).
[13] P. Kanakis and T. Kamalakis, Opt. Lett. **41**, 1372 (2016).
[14] Z. Deng, X. Shi, C. Tan, and X. Fu, J. Opt. Soc. Am. B **33**, 857 (2016).
[15] A. Demircan, S. Amiranashvili, C. Brée, C. Mahnke, F. Mitschke, and G. Steinmeyer, Sci. Rep. **2**, 850 (2012).
[16] A. Demircan, S. Amiranashvili, C. Brée, F. Mitschke, and G. Steinmeyer, Nonlinear Phenom. Complex Syst. **16**, 24 (2013).
[17] A. Demircan, S. Amiranashvili, C. Brée, C. Mahnke, F. Mitschke, and G. Steinmeyer, Appl. Phys. B **115**, 343 (2014).
[18] C. M. de Sterke, Opt. Lett. **17**, 914 (1992).
[19] N. G. R. Broderick, D. Taverner, D. J. Richardson, M. Ibsen, and R. I. Laming, Phys. Rev. Lett. **79**, 4566 (1997).
[20] B. W. Plansinis, W. R. Donaldson, and G. P. Agrawal, Phys. Rev. Lett. **115**, 183901 (2015).
[21] B. W. Plansinis, W. R. Donaldson, and G. P. Agrawal, IEEE J. Quantum Electron. **52**, 1 (2016).
[22] J. Zhou, G. Zheng, and J. Wu, Phys. Rev. A **93**, 063847 (2016).
[23] B. W. Plansinis, W. R. Donaldson, and G. P. Agrawal, J. Opt. Soc. Am. B **33**, 1112 (2016).
[24] D. V. Skryabin and A. V. Yulin, Phys. Rev. E **72**, 016619 (2005).
[25] A. Efimov, A. V. Yulin, D. V. Skryabin, J. C. Knight, N. Joly, F. G. Omenetto, A. J. Taylor, and P. Russell, Phys. Rev. Lett. **95**, 213902 (2005).
[26] C. M. Arabí, F. Bessin, A. Kudlinski, A. Mussot, D. Skryabin, and M. Conforti, Phys. Rev. A **94**, 063847 (2016).
[27] S. Ramachandran, S. Ghalmi, J. W. Nicholson, M. F. Yan, P. Wisk, E. Monberg, and F. V. Dimarcello, Opt. Lett. **31**, 2532 (2006).
[28] J. H. Lee, J. v. Howe, C. Xu, S. Ramachandran, S. Ghalmi, and M. F. Yan, Opt. Lett. **32**, 1053 (2007).
[29] F. Poletti and P. Horak, Opt. Express **17**, 6134 (2009).
[30] L. G. Wright, W. H. Renninger, D. N. Christodoulides, and F. W. Wise, Opt. Express **23**, 3492 (2015).

[31] L. G. Wright, D. N. Christodoulides, and F. W. Wise, Nat. Photonics **9**, 306 (2015).
[32] L. G. Wright, S. Wabnitz, D. N. Christodoulides, and F. W. Wise, Phys. Rev. Lett. **115**, 223902 (2015).
[33] COMSOL MULTIPHYSICS, https://www.comsol.com/.
[34] J. W. Fleming, Appl. Opt. **23**, 4486 (1984).
[35] J. W. Fleming and D. L. Wood, Appl. Opt. **22**, 3102 (1983).
[36] P. Horak and F. Poletti, *Recent Progress in Optical Fiber Research* (InTech, Croatia, 2012), Chap. 1.
[37] G. P. Agrawal, *Nonlinear Fiber Optics* (Academic, San Diego, 2007).
[38] S. Pickartz, U. Bandelow, and S. Amiranashvili, Phys. Rev. A **94**, 033811 (2016).
[39] L. Tartara, IEEE J. Quantum Electron. **48**, 1439 (2012).
[40] V. V. Afanasyev, Y. S. Kivshar, V. V. Konotop, and V. N. Serkin, Opt. Lett. **14**, 805 (1989).
[41] B. Frisquet, B. Kibler, P. Morin, F. Baronio, M. Conforti, G. Millot, and S. Wabnitz, Sci. Rep. **6**, 20785 (2016).